Available online at www.sciencedirect.com
SCIENCE DIRECT®
ELSEVIER
Applied Surface Science 218 (2003) 188–194
applied surface science
www.elsevier.com/locate/apsusc

Interaction of methanol with Zr(0 0 0 1)

N. Stojilovic, D.W. Weber, R.D. Ramsier*

Departments of Physics, Chemistry, and Chemical Engineering, The University of Akron, Akron, OH 44325-4001, USA

Received 21 February 2003; accepted 11 April 2003

Abstract

Interaction of methanol (CD_3OD) with Zr(0 0 0 1) is studied by temperature programmed desorption (TPD), Auger electron spectroscopy (AES) and secondary electron emission crystal current (SEECC) methods. We find that a 10 K difference in adsorption temperature (150 K versus 160 K) alters the amount of desorbing species with no effect on desorption temperature. Higher adsorption temperature results in lower desorption yield. Regardless of adsorption temperature, methanol desorbs at ~600 K at higher exposures, with almost no desorption at lower exposures. AES reveals a different evolution of carbon and oxygen signals during heating with carbon being left near the surface region and oxygen dissolving into the subsurface/bulk. Variations in crystal current reflect the presence of the adsorbed species.

Keywords: Zirconium; Methanol; Temperature programmed desorption (TPD); Auger electron spectroscopy (AES); Kinetics; Surface

1. Introduction

Zirconium is chemically very reactive with respect to light elements such as H, C, and O and to small molecules containing these constituents. This can be rationalized based on its reduction potential of −1.5 V at standard temperature and pressure, in comparison to metals such as Cu, Ni, or Zn, that have reduction potentials of +0.34, −0.26, and −0.76 V, respectively [1]. In addition, zirconium also has a high affinity for taking these light elements into solid solution. The solid solubility of oxygen in zirconium, for example, goes up to ~30 at.% [2]. Applications of zirconium and zirconium-based alloys are numerous and are usually based on the properties of the oxide films formed on the exposed surfaces. Because of their high refractive index, these oxide films are used as optical coatings. On the other hand, because of a high dielectric constant [3], wide band gap and thermodynamic stability on Si [4], zirconium oxide is being considered as a replacement for SiO_2 as a gate dielectric in transistors. Finally, due to excellent corrosion resistance, zirconium is used in the nuclear industry as a structural material as well as in the chemical and biomedical communities.

Strong agents such as NaOH and H_2S that induce stress corrosion cracking (SCC) in a variety of metals do not affect zirconium. In addition, zirconium is immune to attack by sea water and $MgCl_2$ that cause SCC in stainless-steels [5]. However, the corrosion resistance of this metal is affected by impurities such as carbon, and it is known that zirconium becomes susceptible to SCC when exposed to some organic liquids such as methanol [5]. As part of an effort to understand the behavior of zirconium alloys in the presence of organic compounds, we present a study of

* Corresponding author. Tel.: +1-330-972-4936; fax: +1-330-972-6918.
E-mail address: rex@uakron.edu (R.D. Ramsier).

0169-4332/$ – see front matter
doi:10.1016/S0169-4332(03)00584-1

the interaction of methanol (CD_3OD) with Zr(0 0 0 1) under ultrahigh vacuum (UHV) conditions.

Our recent studies of Zr(0 0 0 1) reveal that various species such as water [6], ammonia [7], nitric oxide [8], and oxygen [9] dissociate upon adsorption in the 150–190 K range. Very complex desorption kinetics have been observed in all of these studies that could not be explained by standard desorption models. In the present study, we further investigate the desorption kinetics that this surface exhibits and focus on new features associated with exposure to carbon-containing species.

2. Experimental

All experiments are carried out in a stainless-steel UHV chamber at pressures $\sim 2.7 \times 10^{-8}$ Pa. Detailed descriptions of this UHV system can be found elsewhere [6]. Summarily, the system is pumped by ion getter and titanium sublimation pumps with a liquid-nitrogen-cooled cold trap. A main gate valve separates a turbomolecular pump from the main chamber. The Zr(0 0 0 1) single crystal has cylindrical shape with a thickness of 1 mm and a radius of 3 mm. One side of the crystal is polished to 0.03 μm and has an uncertainty in orientation less than 1°. Two thermocouples (type-E) spot-welded to the sample are part of a temperature-controlled feedback loop. Tantalum wires spot-welded to the sample provide dc heating and a copper braid connected to a liquid-nitrogen cold finger provides cooling of the sample.

Sample cleaning is carried out by 2 h sputtering cycles (2 keV, 2 $\mu A/cm^2$) followed by annealing to 840 K for 2 min. This is done after each exposure to methanol until the C (KLL, 272 eV)/Zr (MNN, 94 eV) and O (KLL, 512 eV)/Zr (MNN, 94 eV) Auger ratios return to the ''clean'' surface values [10]. The reactive nature of zirconium makes it nearly impossible to achieve and maintain an atomically clean surface with respect to oxygen and carbon without using higher annealing temperatures. This will be discussed in later sections. Methanol-d_4 (*D*, 99.8%) is introduced into the chamber from a glass bulb through a stainless-steel gas handling system using a precision leak valve. The turbomolecular pump is used for pumping the gas line prior to every experiment. Methanol is purified by freeze–pump–thaw cycles and the purity of the dosing gas is monitored by a quadrapole mass spectrometer (QMS). Backfilling is carried out at two different temperatures, 150 and 160 K. All methanol cracking fragments detected during backfilling are also observed in temperature programmed desorption (TPD). No 44 amu (CO_2) or other unexpected signals are observed during exposure or TPD.

During backfilling and TPD, *m*/*e* values are monitored by the QMS positioned in line-of sight to the sample surface. The heating rate during TPD is 1.8 K/s. To avoid systematic errors, exposures to methanol are performed in random order. The secondary electron emission crystal current (SEECC) measurements [11,12] are performed using the Auger electron gun (3 keV, 15 $\mu A/cm^2$). Auger electron spectroscopy (AES) and SEECC data are collected at 150 K after stepwise annealing, which is performed with the same heating rate as in TPD. SEECC values are taken before each Auger scan using an ammeter connected in series between ground and the sample.

3. Results and discussion

Decomposition of methanol on various transition metal surfaces has been reported and higher temperatures are found to stimulate decomposition of this molecule. Following adsorption at 100 K it dissociates on Pt(1 1 1) above 140 K to carbon monoxide and hydrogen atoms [13], but is found to be stable on Ni(1 1 0) surfaces up to ~150 K [14]. A recent study of adsorption at 153 K on TiC and VC(1 0 0) surfaces reveals that methanol evolves during heating through molecular and recombinative desorption channels [15]. Room temperature adsorption on ZrC(1 0 0) is found to be molecular whereas on ZrC(1 1 1) it is dissociative [16]. Study of CH_3OH on Al(1 1 1) [17] reveals the formation of methoxy species during heating multilayers to ~170 K, which then decompose upon further heating and desorb as CH_4 and H_2. Here, it was reported that the work function of aluminum decreases significantly upon methanol adsorption and that oxygen is left on the surface after annealing.

Isotopic (CD_3OD) methanol is chosen in the present study so that overlap of possible O_2^+ and CH_3OH^+ 32 amu signals is avoided. Detected 36 amu signals in our experiments are therefore due to desorption of CD_3OD^+ species only, and we do not find evidence for oxygen desorption. Fig. 1 shows a set of 36 amu spectra

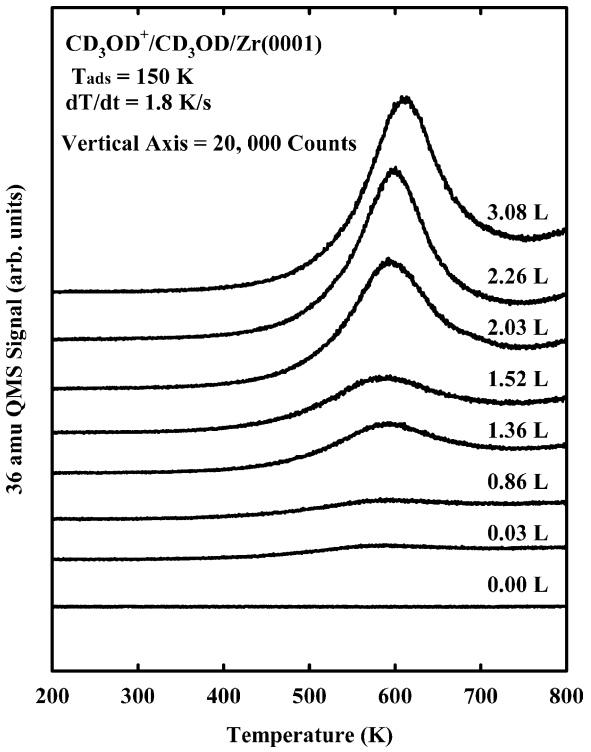

Fig. 1. Methanol (CD_3OD^+) TPD spectra following 150 K methanol adsorption on Zr(0 0 0 1) surfaces.

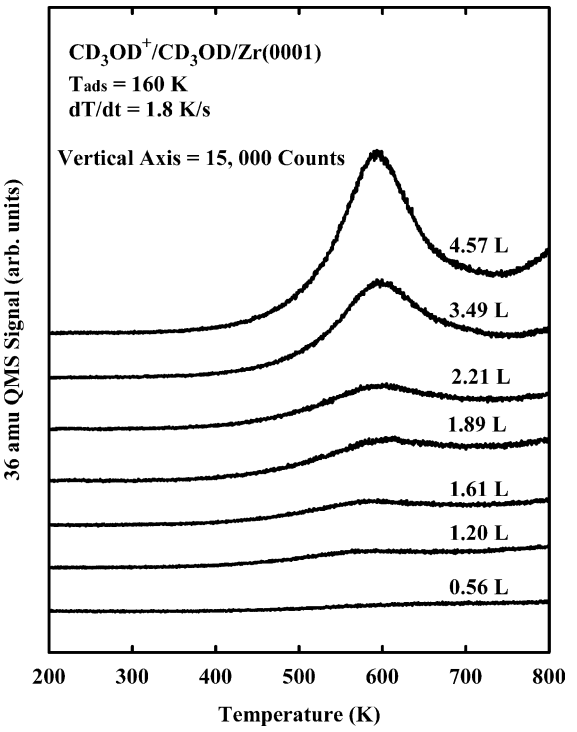

Fig. 2. Methanol (CD_3OD^+) TPD spectra following 160 K methanol adsorption on Zr(0 0 0 1) surfaces.

during TPD following methanol adsorption at 150 K. Exposures below 1 L (1 L = 1.3×10^{-4} Pa s) produce essentially no desorption of methanol due to decomposition during formation of the first monolayer(s). At larger exposures, an increase in desorption yield with exposure is observed with a desorption peak maximum at about 600 K. Fig. 2 presents desorption spectra following backfilling at 160 K. An increase in adsorption temperature of 10 K does not alter desorption temperatures significantly as in the case of exposure to nitric oxide [8] or ammonia [7], but only results in desorption yield changes. CD_3OD desorption yields for these two temperatures are presented in Fig. 3. This figure shows that greater desorption yields occur for lower adsorption temperatures. This can be explained based on the sticking coefficient of methanol on Zr(0 0 0 1) and on decomposition of this molecule upon adsorption. The sticking coefficient is higher at lower temperature whereas higher temperature causes more dissociation. However, it is unknown at present which factor contributes more in our data.

These methanol data indicate relatively simple desorption kinetics without participation of subsurface/bulk species previously observed after exposure of Zr(0 0 0 1) to NH_3 and NO [7,8]. Earlier we found that by varying adsorption temperatures we could alter desorption temperatures in such a way that a higher adsorption temperature resulted in a lower desorption temperature. Higher adsorption temperatures also resulted in greater TPD yields of species desorbing from Zr(0 0 0 1) surfaces. A phenomenological model accounting for these observations has been proposed [18]. It assumes decomposition of adsorbing species and partial exchange of surface and subsurface/bulk species (N, O and H). Relatively broad desorption features have been rationalized by diffusion-driven desorption mechanisms in these previous cases. Accordingly, the relatively sharp desorption features of methanol indicate that surface species play a major role in desorption kinetics that are not limited by subsurface diffusion. Based on first-order desorption kinetics and assuming a value for the pre-exponential

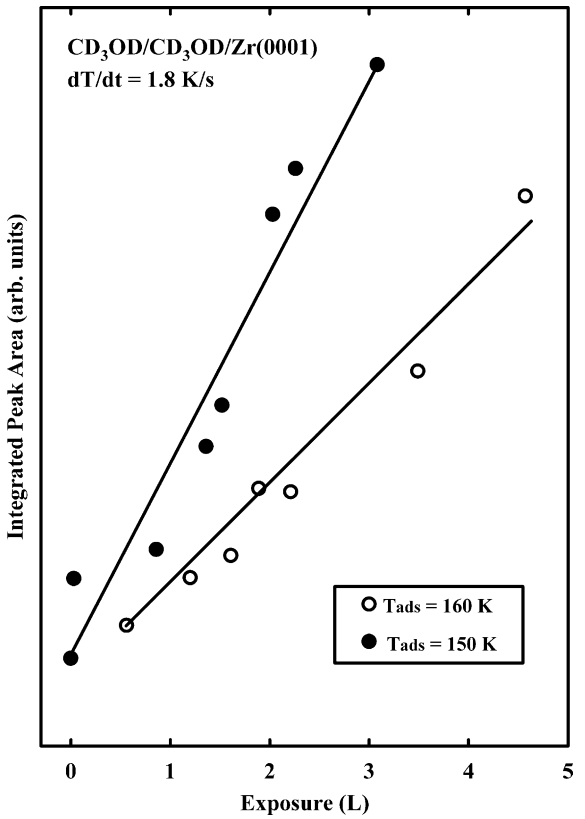

Fig. 3. Integrated methanol desorption yields from Zr(0 0 0 1) surfaces after CD_3OD adsorption at 150 K (solid points) and 160 K (hollow points).

factor of 10^{13} s^{-1}, we calculate the activation energy for desorption of methanol to be ~160 kJ/mol at higher exposures.

Based on our AES and SEECC measurements, we propose that in the present case carbon remains in the near surface region after TPD. This is consistent with a study of CO on polycrystalline zirconium that revealed carbon occupying the region just beneath the outermost zirconium layer [19]. It is reasonable to assume that carbon alters the activation energy for bulk/surface diffusion, which would explain why we find no evidence of significant mass transport effects in TPD. It is important to note that we observe no shifts in the Zr Auger features that would indicate surface oxidation during our experiments with methanol.

We compare C (KLL, 272 eV) and O (KLL, 512 eV) Auger peak-to-peak heights (APPH) (not shown) to that of the Zr (MNN, 94 eV) transition. Auger ratios defined as $R_c = C$ (KLL)/Zr (MNN) and $R_o = O$ (KLL)/Zr (MNN) are determined from spectra collected at ~150 K after stepwise annealing. After exposing Zr(0 0 0 1) to CD_3OD, the surface concentration of carbon and oxygen increases. During stepwise heating the carbon concentration does not seem to vary significantly up to 800 K. Oxygen behaves similarly during annealing but above 700 K a sudden decrease in the concentration of surface oxygen is observed. The same trend has been observed for various exposures, and indicates that oxygen can overcome the carbon-related activation barrier for subsurface diffusion above 700 K. This decrease in the concentration of surface oxygen upon annealing reflects desorption as seen by TPD and oxygen diffusion into the bulk as has been reported by others [20,21]. Carbon, like oxygen, also diffuses into the bulk at high temperatures but with much lower diffusion rates [20]. Our annealing temperatures leave some carbon on the surface but on the other hand prevent outward sulfur segregation.

Methanol undergoes decomposition during formation of the first layer and the major TPD yield most likely comes from the second adsorbed layer that contains more molecular than atomic species. Since exposures up to ~1 L result in practically no desorption even for lower adsorption temperature we conclude that methanol decomposes upon formation of the first layer thus increasing the concentration of surface carbon. This can be seen in Fig. 4a where after exposure to only 0.38 L of methanol annealing to 800 K still leaves carbon on the surface. Notice that the C (KLL, 272 eV) feature does not change significantly after exposure and within experimental uncertainties it is difficult to see much difference in the peak-to-peak heights of this feature before and after exposure. However, the Zr (MNN, 94 eV) feature also changes after exposure so that the carbon versus zirconium ratio jumps from $R_c = 0.23$ (before exposure) to 0.29 (after exposure). After annealing to 800 K, possibly due to rearrangement of the surface adatoms and some desorption/diffusion, the signal-to-noise ratio improves and the presence of carbon is clearer. We see that annealing to 800 K returns the oxygen concentration to the ''clean'' surface value whereas carbon removal requires sputtering.

In Fig. 4a and b the presence of impurities (C and O) on the Zr(0 0 0 1) surface prior to exposure is clear.

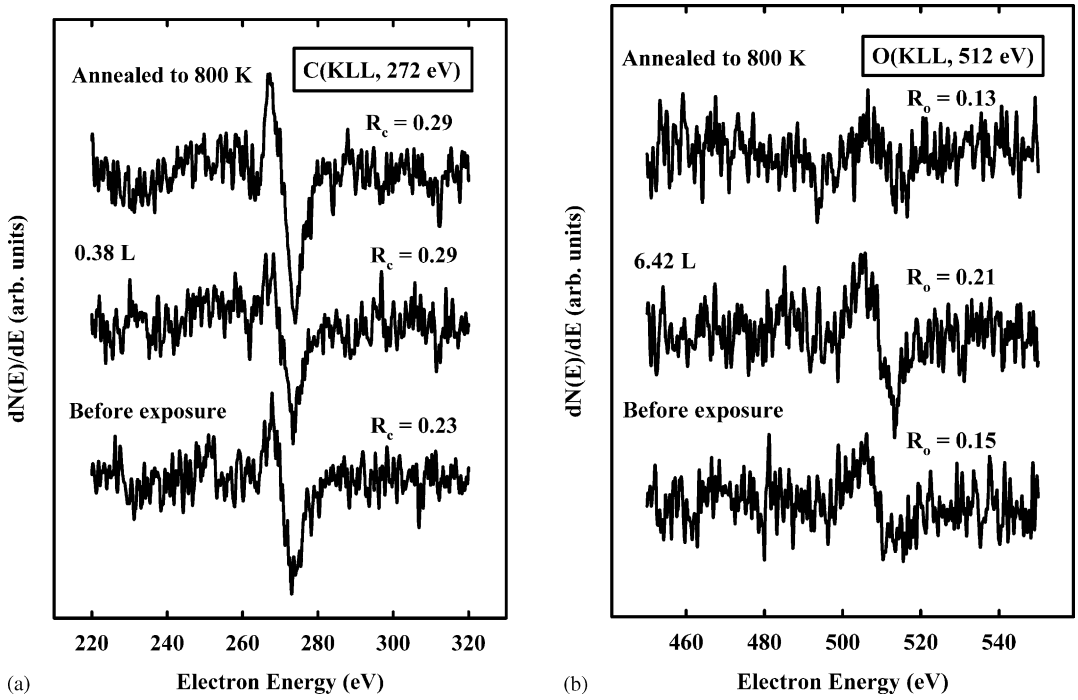

Fig. 4. Derivative mode Auger features: (a) C (KLL, 272 eV) before exposure, after exposure to 0.38 L methanol, and after annealing to 800 K; (b) O (KLL, 512 eV) before exposure, after exposure to 6.42 L methanol, and after annealing to 800 K. All data are taken at ~150 K following stepwise annealing.

This is expected for the surface of a reactive metal such as zirconium. The behavior of zirconium surfaces exposed to various gases is complex and sensitive to the presence of impurities. The presence of sulfur, for example, influences oxygen adsorption and lowers its sticking coefficient [22]. It has been reported that surface sulfur has a much stronger effect on chemisorbed oxygen than vice versa [23]. We keep our annealing temperature below 900 K to prevent sulfur segregation to the surface and thus reduce its effects on the adsorption of methanol. The behavior of hydrogen during heating differs from that of carbon and oxygen. Heating to high temperatures results in hydrogen desorption rather than diffusion into the bulk [20]. The fact that different subsurface/bulk impurities diffuse to the surface at different temperatures plus the high reactivity of zirconium with respect to background gases are major problems in obtaining impurity-free surfaces.

Even though our annealing temperatures are low enough to prevent sulfur segregation, carbon and oxygen are still present on the Zr(0 0 0 1) surfaces. Our nominally clean surface can be characterized by $R_c \sim 0.21$, $R_o \sim 0.15$ and R_{Zr} = Zr (MNV)/Zr (MNN) ~ 0.9. These ratios are different from those that have been reported by other groups. For example, one group [21] characterized clean Zr(0 0 0 1) with $R_c = 0.00$, $R_o = 0.00$, and $R_{Zr} = 1.40$. By applying slightly higher annealing temperatures, these authors managed to reduce concentrations of surface carbon and oxygen below what we achieve. It should be noted that the S (LMM, 152 eV) feature overlaps with the Zr (MNV, 148 eV) transition making distinction between them difficult. Our preliminary experiments (not shown) on SO_2/Zr(0 0 0 1) reveal that surface sulfur increases the Zr (MNV, 148 eV) Auger feature significantly. Similar results obtained by another group [22] characterize a sulfur-free polycrystalline Zr surface with $R_{Zr} = 1.3$ and with almost no carbon and oxygen present.

Recording the crystal current through the sample under 3 keV electron bombardment, reflects changes in secondary electron emission upon methanol adsorption. Observed changes are probably due to changes in the work function. In Fig. 5, SEECC measurements

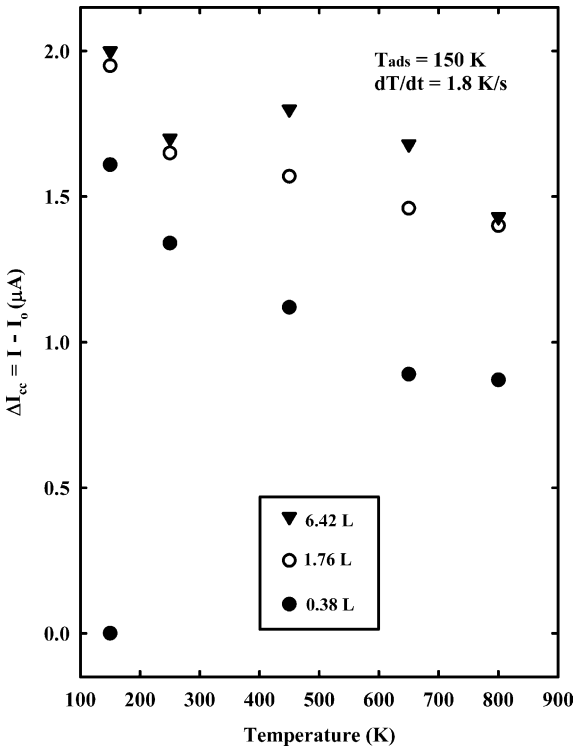

Fig. 5. Changes in crystal current with respect to the initial conditions vs. annealing temperature for three different methanol exposures of 0.38 L (solid points), 1.76 L (hollow points), and 6.42 L (solid triangles) at 150 K.

versus annealing temperature are shown for three different exposures (0.38, 1.76, and 6.42 L) following adsorption at 150 K. Because even very small difference in the position of the sample might affect the crystal current the data are presented as the deviation from the initial crystal current values (I_0). An abrupt change in the crystal current value takes place even after exposure to only 0.38 L of methanol. Subsequent heating reflects how the crystal current depends on the behavior of adsorbed species. Low methanol exposures (<1 L) result in very little thermal desorption while Auger data reveal an increased concentration of carbon and oxygen. We assume that at low exposure SEECC data represent the presence of atomic species (C, O, H) during heating. Analysis of SEECC data for higher exposures is more complicated. This is partly due to the fact that both atomic and molecular species are probably present and also that diffusion into the bulk is accompanied by desorption at ∼600 K.

Fig. 5 also reveals how higher exposures change the shape of the SEECC curve. The measured crystal current depends on a convolution of the carbon, oxygen, and hydrogen concentrations at the surface, $I_{cc} = I_{cc}$(C, O, H). The exact form of this function remains unknown. After exposure to methanol approximately equal amounts of carbon and oxygen atoms are present on the surface and the change in crystal current is caused by the presence of these species and hydrogen. Since our AES data indicate that carbon cannot be removed by annealing, differences in the values of I_{cc} after annealing are attributed mostly to the presence of carbon.

From this study of the interaction of CD_3OD with Zr(0 0 0 1) surfaces, we gain some insight into how carbon-containing species may behave. We have a good indication that carbon elevates the activation energy for bulk/surface diffusion thus preventing mixing of bulk impurities with adsorbed species and resulting in relatively simple kinetics reflected in TPD. Desorption kinetics resemble those of first order and from this an activation energy for desorption has been estimated. These kinetics are very different from what we have previously observed for nitrogen-containing species, and point to a need for further work. We believe that a thorough understanding of organic molecules on zirconium surfaces is important for developing a comprehensive picture of this class of materials, which is one of our goals.

4. Conclusions

We observe that unlike nitrogen and oxygen, carbon does not mix with bulk impurities but upon CD_3OD decomposition stays in the near surface region. TPD data indicate that desorption yields depend on adsorption temperature but that desorption temperatures are unaffected. This is due to lower sticking coefficient and greater probability of dissociation at higher adsorption temperature. TPD data indicate that mainly surface species participate in thermally induced desorption with no or very little contribution from bulk impurities. This is due to the presence of carbon, which elevates the activation energy for bulk/surface diffusion below 600 K. AES reveals that following CD_3OD adsorption, subsequent annealing to temperatures above 600 K activates oxygen diffusion into the

bulk leaving carbon on the surface. SEECC measurements reflect the surface condition upon methanol adsorption and subsequent stepwise heating. For low exposure, where practically no desorption is observed in TPD, the crystal current changes reflect oxygen diffusion into the bulk. After higher exposures, the changes in SEECC data during heating also reflect changes in the surface coverage caused by methanol desorption at ∼600 K.

Acknowledgements

Acknowledgement is made to the Donors of the American Chemical Society Petroleum Research Fund for partial support of this research.

References

[1] D.R. Lide (Ed.), CRC Handbook of Chemistry and Physics, 83rd ed., Chemical Rubber Company, CRC Press, Cleveland, Ohio, USA, 2002–2003.
[2] T. Tanabe, M. Tomita, Surf. Sci. 222 (1989) 84.
[3] G.D. Wilk, R.M. Wallace, J.M. Anthony, J. Appl. Phys. 89 (2001) 5243.
[4] K.J. Hubbard, D.G. Schlom, J. Mater. Res. 11 (1996) 2757.
[5] T.-L. Yau, in: R.H. Jones (Ed.) Stress-Corrosion Cracking, ASM International, Materials Park, Ohio, USA, 1992 (Chapter 11).
[6] Y.C. Kang, M.M. Milovancev, D.A. Clauss, M.A. Lange, R.D. Ramsier, J. Nucl. Mater. 281 (2000) 57.
[7] Y.C. Kang, R.D. Ramsier, Vacuum 64 (2002) 113.
[8] Y.C. Kang, R.D. Ramsier, J. Nucl. Mater. 303 (2002) 125.
[9] Y.C. Kang, R.D. Ramsier, Appl. Surf. Sci. 195 (2002) 196.
[10] N. Stojilovic, Y.C. Kang, R.D. Ramsier, Surf. Interface Anal. 33 (2002) 945.
[11] C. Argile, G.E. Rhead, J. Phys. C: Solid State Phys. 30 (1982) L193.
[12] R.D. Ramsier, K.-W. Lee, J.T. Yates Jr., Langmuir 11 (1) (1995) 169.
[13] B.A. Sexton, Surf. Sci. 102 (1981) 271.
[14] S.R. Bare, J.A. Stroscio, W. Ho, Surf. Sci. 150 (1985) 399.
[15] P. Frantz, S.V. Didziulis, L.C. Fernandez-Torres, R.L. Guenard, S.S. Perry, J. Phys. Chem. B 106 (2002) 6456.
[16] T. Nakane, T. Noda, K. Ozawa, K. Edamoto, Surf. Sci. 433–435 (1999) 180.
[17] S.A. Sardar, J.A. Syed, K. Tanaka, F.P. Netzer, M.G. Ramsey, Surf. Sci. 519 (2002) 218.
[18] Y.C. Kang, R.D. Ramsier, Surf. Sci. 519 (2002) 229.
[19] G.B. Hoflund, G.R. Corallo, D.A. Asbury, R.E. Gilbert, J. Vac. Sci. Technol. A 5 (1987) 1120.
[20] J.S. Foord, P.J. Goddard, R.M. Lambert, Surf. Sci. 94 (1980) 339.
[21] J.R. Lou, P.C. Wong, K.A.R. Mitchell, Can. J. Chem. 66 (1988) 3157.
[22] K. Ojima, K. Ueda, Appl. Surf. Sci. 165 (2000) 141.
[23] P.C. Wong, K.A.R. Mitchell, Can. J. Chem. 64 (1986) 2409.